

Analysis of the Impedance Behaviour for Broadband Dipoles in Proximity of a Body Tissue: Approach by Using Antenna Equivalent Circuits

Tommi Tuovinen^{*}, Markus Berg, and Jari Iinatti

Abstract—Ultra wideband (UWB) antenna operation close to tissue is examined by using lumped-element equivalent circuits in the present paper. The impact of tissue within the reactive near-field of the antenna is introduced in terms of efficiency, impedance and matching to $50\ \Omega$. The parasitic components for the series- and parallel-resonant stages of the equivalent models are proposed for taking the impact of tissue into account on the antenna design. The first time the antenna impedance behaviour is presented in terms of capacitance, inductance and resistance as a function of the radiator distance on the tissue surface for UWB antennas. The capacitance was observed to increase with the distance on the tissue surface by achieving the maximum value close to the reactive near-field boundary. The inductance has the maximum on contact the tissue, decreasing strongly with the first millimetres and remaining constant with the higher distance. The maximum value of input resistance was seen to clearly increase with the distance, having the maximum value in the first third of the studied range, descending close to the value in free space at the boundary at the end. The results are achieved by realising electromagnetic simulations for the antennas and comparing the performance with the operation of the equivalent models.

1. INTRODUCTION

Recent advances in the research of wireless body area networks (WBANs) [1] have enabled wearable technology to be able to become in consumer products. Hopefully, it is a part of people's life in the near future. One significant result of the development work is the publication of the international IEEE standard 802.15.6 [2] in early 2012 for the short range body area transmissions. Some possible applications for BAN are, for instance, health monitoring by using medical sensors or sport tracking for, e.g., acceleration records. In future, a range of devices of a person to carry is assumed to increase, which is partly because of wearable electronics, since those are likely constantly-connected-type of applications. The key issue of the convenience of such a usage without wired connections around a body is possible because of antennas, which play a major role in the establishment of a communication system.

In the context of wearability, an antenna is planned to be part of clothing [3] or integrated into an electronic measurement device that is used, e.g., for health recordings. Naturally, the antenna size must be miniaturized, which together with the harmful body effects [1, 4] cause major challenges for the antenna operation. Based on the review to the open literature, many articles report the effect of a user to have a strong impact on the antenna performance, which is seen mainly as detuning the resonant frequency and electromagnetic absorption. Even though these effects have been known, the physical mechanism and behaviour of the wearable antenna on a body has not been comprehensively explained. Wearable communication systems cannot be realized without understanding about the impact of the

Received 19 February 2014, Accepted 4 April 2014, Scheduled 9 April 2014

^{*} Corresponding author: Tommi Tuovinen (Tommi.Tuovinen@ee.oulu.fi).

The authors are with the Department of Communications Engineering, Centre for Wireless Communications, University of Oulu, P. O. Box 4500, Oulu 90014, Finland.

changes of an individual antenna operation and their impacts at the link level and finally know how to compensate them. Comprehension of the antenna impedance behaviour is worthwhile in order to predict the performance.

To understand the wearable performance, both the interaction and absorption mechanisms of a body are profitable to acquaint. Related to the latter, some examinations have been recently reported of body energy-absorption [4, 5] and standing wave effect of a body [6]. Especially, the finding of Kivekäs et al. in [5] is particularly interesting: peak specific absorption rate (SAR) values are not actually related to the antenna current distributions, as it has been commonly believed. Instead, the mechanism lies in the fact that the maximum SAR can be inspected with the real part of tissue's permittivity and its impact on the electric-field components with respect to the tissue surface. The authors have earlier considered the effect of tissue combinations and tissue layer thicknesses on a wearable antenna performance in [7], based on the values in [8]. It was concluded that the maximum SAR values vary with different tissue compounds. These results indicate that the proper understanding about the antenna alignment on a body has clear influence on the entire wearable system performance. In addition to the on-body antenna position, the distance on a body surface has been reported having a significant impact on the performance [6, 9, 10]. A natural issue causing variations for the distance on a body is clothing, which might change the wearable device positions on a body, thus should be taken into account in a design. Also the bendable features [11] might be required for an antenna because of 1) a body shape, 2) integration to clothing or 3) the natural movements of a human.

Challenges of the wearable antenna design arise due to the presence of a lossy tissue and of its impact on impedance characteristics, pattern shape and current distributions. Neglecting these result in the lack of available radiation performance at the end. Keeping the practical use scenarios and applications in mind, some relevant questions related to the antenna alignment on-body are 1) how far the antenna can be spaced on a body in reality, 2) what are the dimensions of areas available for the antenna radiators, 3) which parameters a sensor(s) of a wearable device will be used to measure, 4) what are the restrictions for the antenna use distance on a body based on the interaction mechanism and propagation, and so forth. At the end, there are many factors affecting both on the antenna use distance and the final antenna concept of any wearable device. Some authors have been investigated the time domain behaviour for wearable UWB antennas [12, 13]. In addition, related to the best use position/distance on-body, studies in [1, 9] have concluded that when no body tissues are in the range of the closest space surrounding an antenna (i.e., within reactive near-field [14, 15] or Wheeler's radiansphere [16]), achievable performance can be relatively close to that of up to free space. However, the boundary of the field is challenging to explain unambiguously, because of the changes in fields happen gradually [17]. Further, it should be understood that the reactive proportion of the near-field does not radiate. Nevertheless, it is the important proportion of the radiation mechanism [17]. We assume that the most of the wearable antennas will be used in the said range, which is the content of the present paper to examine.

In this study, in line with our previous referred research work on the investigations of antenna-body interaction mechanism in [7, 9, 16], we wish to present the investigation of the impact of tissue within the reactive near-field of wearable broadband antennas. Several type of antennas have been reported for wearable connections, and probably most of them are monopoles or patches structures, e.g., in [3, 11]. Since the aim of the present paper is to examine the interaction and physical behaviour between an antenna and tissue, we have chosen four representatives for investigations. The antennas are traditional broadband dipoles covering either bandwidth ≥ 500 MHz or the entire Federal Communication Commissions' (FCC) [19] ultra wideband (UWB) [20] of 3.1–10.6 GHz. This is because many antennas can be analysed based on the operation of a dipole and therefore the results of this study can be extended and applied further. The suitable lumped-element equivalent circuit models are utilized to explain the physical antenna behaviour in the presence of tissue. Equivalent circuits are proposed to use for the evaluation of impedance characteristics especially for wearable antennas, since 3D simulations might be time consuming. In addition, one transient provides the antenna operation at one distance on a body. Therefore, it is successful to derive the antenna physical behaviour as a function of the distance on-body. The deeper insight on operation is then provided and saving of time. The clear advantage of equivalent circuits is that the antenna behaviour can be understood in detail. It is recommended to use equivalents also for the investigation and analysis of the physical behaviour

of a bendable wearable antenna.

All simulations (including antennas and circuit verification for equivalent models) in this paper are carried out with Computer Simulation Technology (CST) [21] Microwave Studio (MWS) and Design Studio (DS) software packages, which are widely used both in industry and academia.

2. SIMULATION SETUP

2.1. Studied Antennas

Four planar broadband traditional dipole antennas were used in this study, which satisfy the UWB bandwidth definition of ≥ 500 MHz [17,18]. The antennas are designed to investigate on-body phenomena and body interactions, and a 1.6 mm thick FR4 substrate is used with them. Three antennas produce a single-resonant and are designed for centre frequencies f_c of 3 GHz, 6 GHz and 9 GHz in free space such that their -10 dB S_{11} bandwidths are 500 MHz, 1000 MHz and 1500 MHz, respectively, as shown on Table 1. The 4th antenna is to cover the entire FCC UWB band of 3.1–10.6 GHz. These antennas are originally introduced in [23].

Table 1. Description for the bandwidth of studied single-resonant antennas.

parameter	Antenna		
	3 GHz	6 GHz	9 GHz
centre frequency f_c [GHz]	3.0	6.0	9.0
lower -10 dB S_{11} band edge [GHz]	2.81	5.57	8.35
higher -10 dB S_{11} band edge [GHz]	3.29	6.60	9.99
-10 dB S_{11} bandwidth [MHz]	≈ 500 MHz	≈ 1000 MHz	≈ 1500 MHz
fractional bandwidth f_B [%]	18		

2.2. Tissue Phantom

The user wearing a wearable antenna is known to cause shifts for the resonance frequency of antenna due to the features of lossy tissue, and the impact can be explained with the perturbation theory [24]. In this study, we use the common way in the field as we assume that human body tissue can be modelled as a dielectric object [22] by defining relative permittivity ϵ_r and conductivity σ or loss tangent $\tan \delta$. Electric parameters for a phantom are defined for one tissue [25], which is commonly used way in the open literature. Usually, the dielectric definitions of tissue state that ϵ_r of lossy dielectric material is somewhere 30–45, i.e., clearly higher than air. The material permeability is equal to one, meaning non-magnetic. This indicates the electric parameter to be the key material for the determination of electromagnetic fields in a body [26], and the impact of a dielectric material on the antenna operation can be concluded to be analysed only with the electric fields [27]. We use the dielectric values for the outermost tissue of a body since it has the strongest impact on the performance [7]. Since broadband antennas are studied, the variations of tissue phantom properties with the frequency are taken into account by determining Debye 2nd order dispersion for UWB according to [28,29]. It is supposed that the effect of curvature-shaped body can be mitigated since the studied broadband antennas are physically small. Because of the mentioned reasons, we use a square slab phantom with the infinite size of $40 \times 40 \times 3$ cm³, and the antenna is aligned on top of it while the distance D_{A-S} on the model is varied as shown in Figure 1.

2.3. Discussion about Simulation Approach

Since the scope of this work is with the broadband antennas and their physical behaviour by using equivalent circuits close to tissue phantom, the study is fundamentally based on the simulations. The final determination of circuits is empirical-based, because the equivalents are based on the data aggregated from antenna simulations.

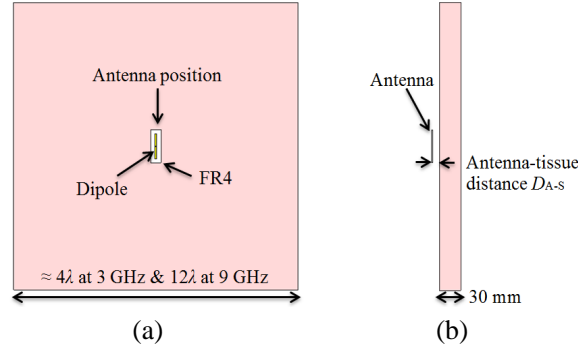


Figure 1. (a) Top view and (b) side view of square slab phantom object and the single-resonant 3 GHz dipole of the studied antennas. Figures indicate the size of tissue model, antenna position and definition of antenna-tissue distance.

It should be understood that it is not relevant to cable and measure the studied balanced antennas because of the well-known cable effect, which changes the antenna impedance causing the equivalents being valid no longer. Naturally, the balun can be used, but without eliminating the confusion, i.e., the antenna feeding cable. The cable will not exist in the real application where the situation is more likely as with the discrete port in simulations. It should not be ignored that the accuracy of current simulators is high. In addition many studies of the correlation between simulations and measurements have been carried out in the long term. Quite often, the problem with the correlation seems to be arisen because of the prototype rustled up in a hurry, thus not being exactly equal with the simulation concept. Another aspect in the advantages of simulations is that as the frequencies get higher, the size of antenna structures decreases, being practically work with the changes of millimetre as in UWB or even with micrometre. Findings of the changes in that level are impossible to realize by prototyping with copper tape.

3. EFFICIENCY AND MATCHING BEHAVIOUR FOR WEARABLE ANTENNA

In this part, the impact of the tissue phantom in the region of the reactive near-field boundary of a wearable antenna is investigated in terms of efficiency and matching characteristics. The behaviour is examined by considering the studied antennas at the different distances D_{A-S} on the tissue model for the mentioned range. The authors believe that most wearable antennas in the real applications will be used on the distances smaller than the size of the reactive near-field.

As introduced earlier, antenna field boundaries cannot be determined unambiguously, but can be approximated. In theoretical books, antennas made of thin wires are often considered, which might not be feasible in practise. The operation of very thin antenna can be estimated, but it should be understood that then 1) radiation characteristics are sensitive to frequency [14], and 2) the bandwidth is the parameter dictating the degree of the change with the frequency. The closest space that surrounds an antenna is called as reactive near-field region, usually marked by R_1 and can be found, e.g., in [14]. For a very short dipole or equivalent [14], i.e., electrically small antenna (ESA) [15], the radius of Wheeler's radiansphere R_W can be used [16]. In the case of R_W , the boundary distance is measured from the antenna surface. According to these, reactive-near field boundary can be calculated either with the largest antenna structure or by Wheeler's radiansphere. The results of calculations are presented for the studied antennas on Table 2 together with the values for free space wavelength. Note that the distance D_{A-S} is announced from the top of tissue surface up to the bottom of antenna substrate. Therefore, a 1.6 mm thick substrate slightly increases the distance further.

3.1. Antenna Radiation Performance

Total antenna efficiency behaviour is shown as a function of D_{A-S} on the tissue model in this part. The results are shown in Figure 2, where each graph is plotted for the range of reactive near-field based on

Table 2. Reactive near-field boundary and Wheeler’s radiansphere for the broadband single-resonant and multi-resonant dipole antennas.

parameter	antennas		
	3 GHz	6 GHz	9 GHz
wavelength λ in free space [mm]	99.7	49.8	33.2
wheeler’s radiansphere R_w [mm]	15.9	7.9	5.3
for single-resonant dipoles			
largest antenna dimension D_L [mm]	34.8	15.9	10.3
reactive near-field boundary R_1 [mm]	12.7	5.6	3.6
for multi-resonant dipole			
largest antenna dimension D_L [mm]	32.6		
reactive near-field boundary R_1 [mm]	11.6	16.4	20.0

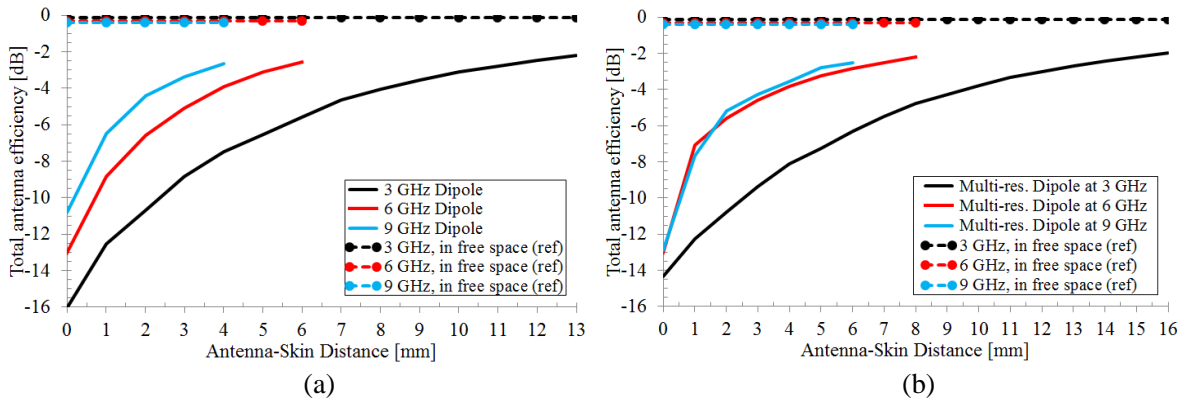


Figure 2. Total antenna efficiency behaviour in the closeness of the tissue surface for the range of (a) reactive near-field boundary R_1 for the single-resonant dipoles, and (b) Wheeler’s radiansphere R_W for the multi-resonant dipole at the frequencies of 3 GHz, 6 GHz and 9 GHz.

the definitions on Table 1. The dashed lines with additional circles present the free space performance. Comparing the results, the lowest frequencies can be observed to suffer more of the lossy tissue in the antenna proximity in comparison with the higher frequencies. This operation is actually not surprising, but is foreseeable. It is observed that the absorption to tissue has the strongest impact on the reduced efficiency. In addition, the deteriorated matching has an impact.

The more interesting is to distinguish that the impact of increase of the first millimetres for the single-resonant dipole on-body has not the clear difference on the absolute improvement on efficiency, e.g., the increase of D_{A-S} from 0 to 3 mm for single-resonant dipoles in Figure 2(a) improves the efficiency 7.2 dB (3 GHz), 7.9 dB (6 GHz) and 7.5 dB (9 GHz). This means the change of efficiency remains almost constant with increased D_{A-S} . Another interesting observation is the similarity between the antenna radiation performances at the boundary of the approximated reactive near-field: the absolute values of -2.2 dB (3 GHz), -2.6 dB (6 GHz) and -2.6 dB (9 GHz) are read from the simulation data, which corresponds to the deterioration of 2.1 dB, 2.3 dB and 2.2 dB of the efficiency in comparison with that of observed in free space. For the multi-resonant antenna, the behaviour is slightly different as the corresponding increase of D_{A-S} from 0 to 3 mm, which improves the efficiency of multi-resonant dipole 5.0 dB (at 3 GHz), 8.4 dB (at 6 GHz) and 8.6 dB (at 9 GHz). This clearly indicates the bottleneck of excellent wearable broadband antenna, i.e., the performance of the lowest band to cover and radiate efficiently. Comparing the results with the Table 1, the multi-resonant seems to behave more likely according to the R_W . The effect of a substrate has also impact on the difference between different

frequencies. We concluded that a strong absorption close to tissue together with the possible changes in the surface currents due to a body are the dominant factors causing the presented behaviour in the vicinity of tissue. However, the deteriorated antenna matching has an influence as well.

Figure 3 compares the currents of the antennas in the situations, where the antenna is in free space (Figures 3(a), 3(d), 3(g), 3(j), 3(m), and 3(p)), aligned on contact with the tissue

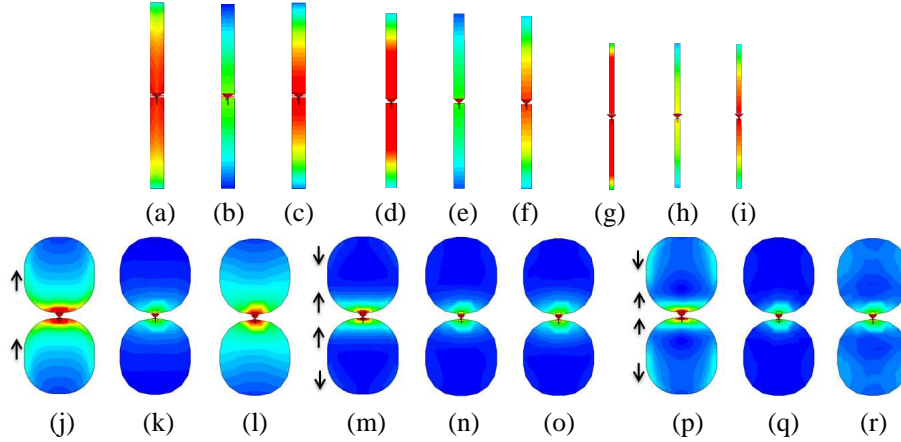


Figure 3. Simulated instantaneous current distributions [A/m] at 0° phase of the studied (a), (b), (c) 3 GHz, (d), (e), (f) 6 GHz, and (g), (h), (i) 9 GHz single-resonants for use cases: (a), (d), (g) in free space, (b), (e), (h) on contact with the tissue, and (c), (f), (i) at the boundary of reactive near-field. The following figures are for multi-resonant at (j), (k), (l) 3 GHz, (m), (n), (o) 6 GHz and (p), (q), (r) 9 GHz, (j), (m), (p) in free space, (k), (n), (q) on contact with the tissue, and (l), (o), (r) at the boundary of R_W , i.e., 3 GHz = 16 mm, 6 GHz = 8 mm and 9 GHz = 6 mm. The colour range is a logarithmic through the range from 0 A/m (blue) to 20 A/m (red).

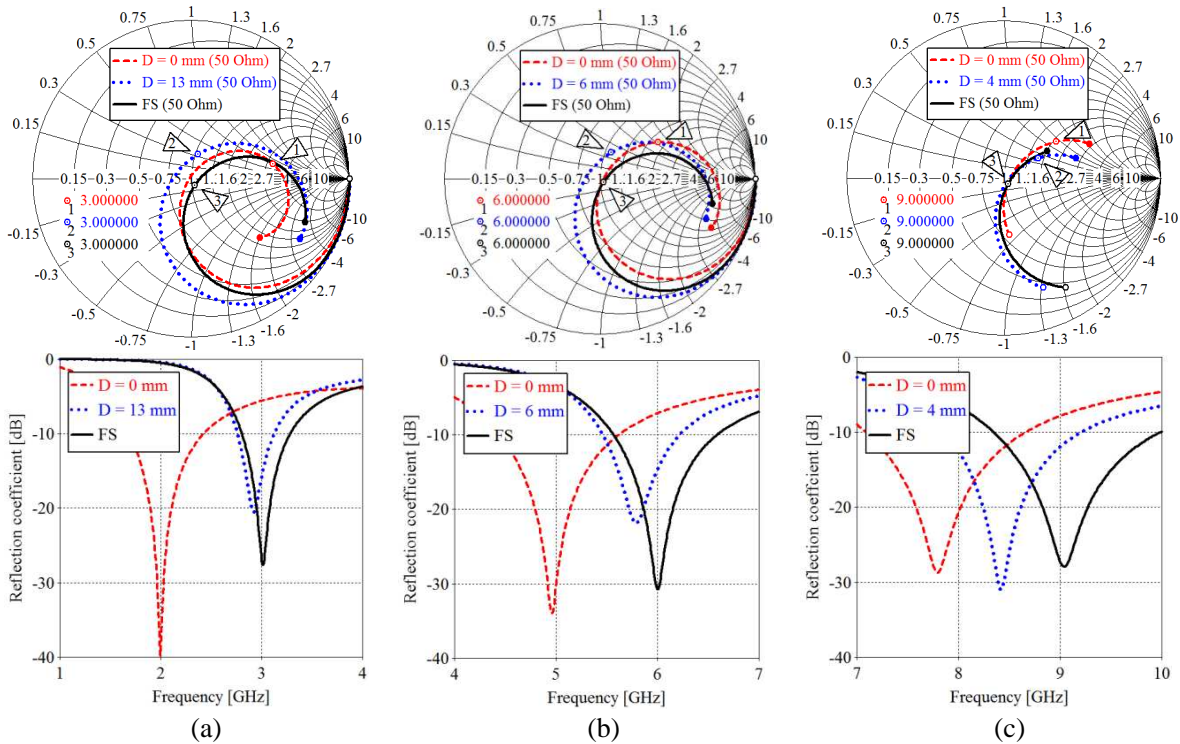


Figure 4. Antenna matching behaviour in free space (FS), on contact with tissue ($D = 0$ mm) and in the boundary of reactive-near field R_1 for single-resonant dipoles at (a) 3 GHz, (b) 6 GHz, and (c) 9 GHz.

(Figures 3(b), 3(e), 3(h), 3(k), 3(n), and 3(q)) and at the boundary of reactive near field (Figures 3(c), 3(f), 3(i), 3(l), 3(o), and 3(r)). The arrows are included to indicate the direction of currents. In each current plot, the same amount of power is fed to the antenna hence the amount of absorption is clearly visible on the contact situation. It is interesting to observe that the currents of single-resonant dipoles at the boundary of reactive near-field obey closely the shape of free space. Naturally, the magnitude slightly differs that is understandable, since the tissue is still nearby, and some proportion of the power causes absorption as far as tissues are visible for an antenna. The more complicated is to analyse the performance of the multiple frequency points of broadband multi-resonant dipole against the theoretical limits. This is because the different parts of antenna radiate with the frequency. In addition, 2nd order wavemode is introduced from 6 GHz upwards. However, the fashion of distributions is similar with single-resonant dipoles. It is visible that the currents have the maximum in the feeding and they travel along the curvature edges of the dipole plates in free space. Strong absorption is faced on contact usage and the current transform at the reactive field boundary start to change equal to the free space operation.

3.2. Matching Behaviour

In this part, the aim is to demonstrate the variation of antenna matching for the range of boundaries in terms of reflection coefficient S_{11} and in Smith Chart. The results for the impedance matching in free space (the black solid line), on contact (red dashed) and at the estimated boundary of reactive near-field (blue dotted) for single-resonant dipoles are collected to Figure 4. S_{11} 's below are intended to support the results in the Chart. The reader can observe that the change of the loop in Chart between free space and on contact is not significant, but the frequency point of interest (shown by markers) that

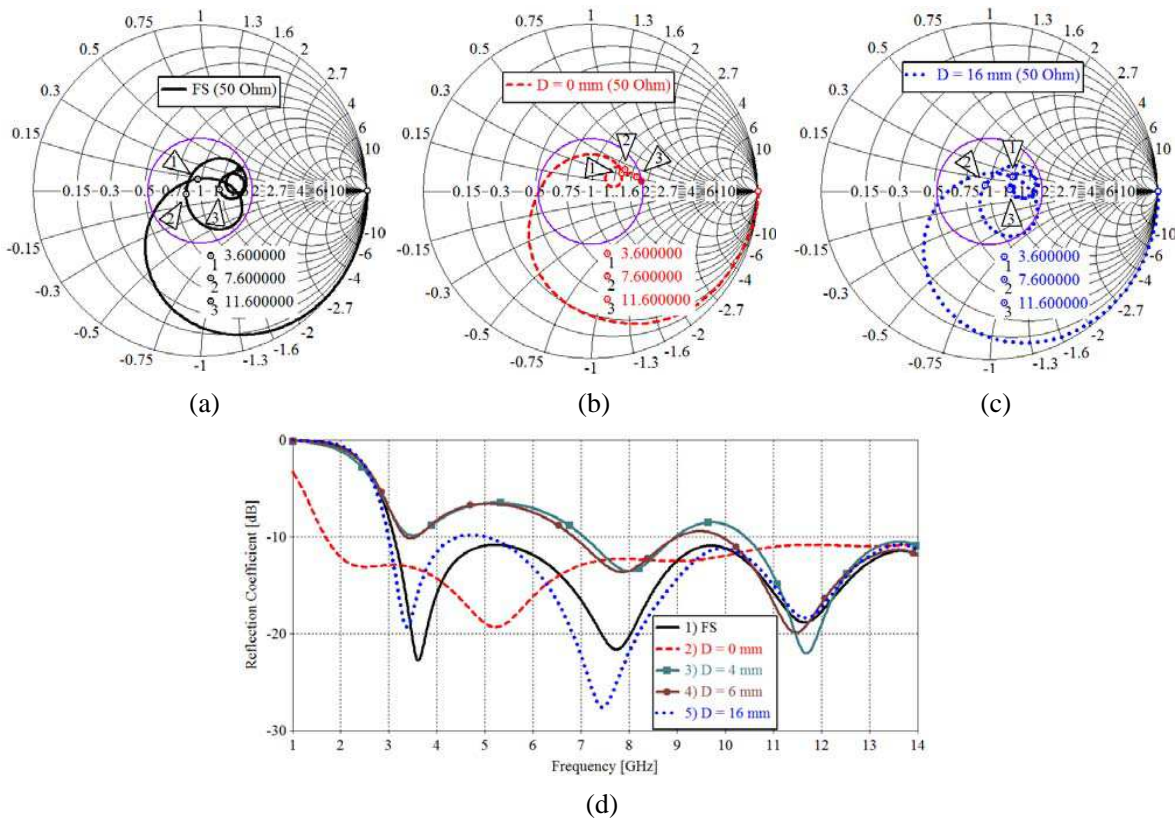


Figure 5. Antenna impedance matching behaviour in Smith Chart (a) in free space (FS), (b) on contact with tissue ($D = 0$ mm) and (c) in the boundary of Wheeler’s radiansphere R_W for multi-resonant with 1st resonance at 3.6 GHz, 2nd res. at 7.6 GHz, and 3rd res. at 11.6 GHz. Figure (d) shows the matching variation for reflection coefficient S_{11} .

is in the midpoint of Chart in free space, notably shifts to the Chart's inductive side. In the case that D_{A-S} is increased, the loop in Chart start to get larger, achieving the maximum size approximately in the third of the approximated size of near-field, by following the shrinkage of the loop when approaching the field boundary.

In practice, the mentioned widening of the loop for the middle of boundary is seen as the poor matching in reflection coefficient in the rightmost subplot of Figure 4, since the Smith's loop has not in the optimum position against the -10 dB area of the Chart, meaning the matching level has changed with D_{A-S} . This indicates that the poor matching has also significant impact on the reduced efficiency. This behaviour is corresponding also for 6 GHz and 9 GHz single-resonant dipoles, but the loop variation is smallish for the 9 GHz, as visible. The multi-resonant dipole is observed to produce three loops in Smith Chart. The largest of them producing the lowest 1st resonance faces the strongest variation with D_{A-S} . The effect of tissue is noticed to change the impedance matching to more inductive as visible between the changes in Figures 5(a)–(b). Figure 5(d) shows clearly how the matching level of the antenna is deteriorated with the first steps of the increased D_{A-S} . The graphs $D = 4$ mm and 6 mm are included to Figure 5(d) to demonstrate this.

4. TISSUE IN THE REACTIVE NEAR-FIELD OF WEARABLE ANTENNA: IMPEDANCE BEHAVIOUR BY EQUIVALENTS

In this section, the antenna input impedance Z_{in} variation for the range of reactive near-field of the broadband dipoles is considered and physical behaviour analysed. Impedance includes input resistance R_{in} , which is the sum of radiation R_r and loss R_L resistances and X_{in} is the input reactance as [14]

$$Z_{in} = R_{in} + jX_{in} = (R_r + R_L) + jX_{in}, \quad (1)$$

by defining the ratio of the voltage to current at antenna terminals in the situation of without any load. Power delivered to the antenna can be maximized when the sum of R_r and R_L is equal to feeding line resistance, and the reactance is the complement for generator's equivalent. The first can be determined with the connection of the radiated power P_{rad} and the maximum currents I_0 [14], or with the ratio of dipole length l and λ [15]

$$R_r = \frac{2P_{rad}}{|I_0|^2} = 20\pi^2 \left(\frac{l}{\lambda}\right)^2. \quad (2)$$

Usually, the length of dipole is reduced to vanish the reactance close to zero [14]. Respectively with (2), the loss resistance R_L can be also defined with the power P_L dissipated on the heat and ohmic losses of the antenna [15] or by taking into account the shape of current distributions, demonstrated in Figure 3, by using the surface resistance R_s [14]

$$R_L = \frac{2P_L}{|I_0|^2} = \frac{l}{P}R_s = \frac{l}{2\pi a} \sqrt{\frac{\omega\mu_0}{2\sigma}}, \quad (3)$$

where P is the perimeter of the cross section of the rod, a is the wire radius, and ω , μ_0 and σ are the angular frequency, permeability in free space and conductivity, respectively. In (3), the connection between loss resistance and the width of dipole is shown.

4.1. Connection between Real Part of Impedance and Equivalent's Parallel Stage, and Impedance Variation

Antenna equivalent circuits are widely accepted to characterize antenna operation [30–36]. This part of the study is the continuation of the earlier study in [23] where the impedance dependency on broadband dipole dimensions by using lumped-element equivalents was introduced. The authors' approach to model the dipoles by equivalents was based on the Hamid's procedure in [33], which was also applied by Wang et al. [30] and Liao et al. [35]. The real part of input impedance can be modelled by a parallel-resonant part as demonstrated in [23], and we concluded that the parallel stage is connected to the formation of the practical dipole plate dimensions. This connection is important to understand especially in the case of broadband antennas, since as the bandwidth is aimed to widen, the antenna must utilize its

available volume by geometry [14] to modify the antenna input impedance conveniently. Particularly, this is crucial for the wearable antenna in the presence of a body tissue, since a body causes additional challenges and trade-off for the maximization of the antenna matching and radiation performance. Since an antenna engineer is interested into maximize the matching, the impedance behaviour in the proximity of tissue must be first understood to be able to optimize the operation.

Because of the clear connection between the plates and the parallel-stage, only the behaviour of parallel-resonant part in the vicinity of the tissue is first considered in this part to keep the study rational. The behaviour of impedance for the real part in (1) is shown within the studied range for the single-resonant dipole at 3 GHz in Figure 6. As it is visible, the Z_{in} peak value which is the maximum of R_{in} in (1) further being the combination of R_r and R_L in (2) and (3), draws a circle (demonstrated with the black solid line) around the free space reference. This behaviour is valid for other studied single-resonant dipoles. Also the resonance peaks of the multi-resonant behave with the same fashion as will be shown in the next section.

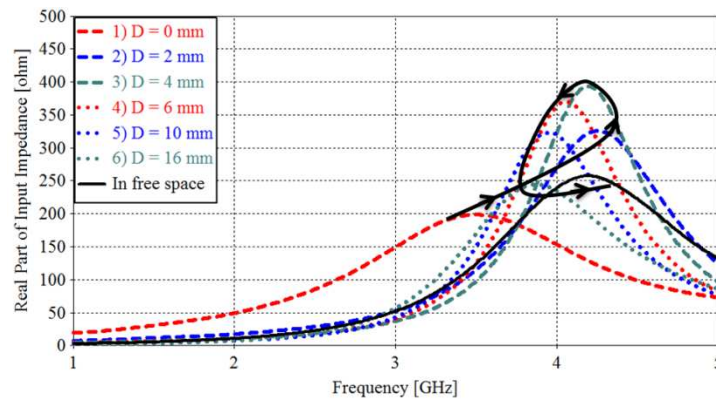


Figure 6. Demonstration of impedance behaviour for the single-resonant dipole at 3 GHz. The black solid line describes the circle that the maximum value of resistance rotates in the studied range.

4.2. Defining Impedance Behaviour by Equivalents in the Vicinity of Tissue

As demonstrated the connection between the antenna dimensions and equivalent, we considered next the required changes for the free space equivalent in order to adapt for the impedance changes in the vicinity of tissue. This was realized by re-defining the component values for capacitance, inductance and resistance. The re-definition was carried out based on the impedance data of dipoles acquired from 3D simulations by following the determination of the proper Z_{in} behaviour for equivalents introduced in [23].

The results are shown in Figure 7 for some distances, because of a large number of the considered values of D_{A-S} . In Figures 7(a), 7(b), and 7(c), the behaviour is shown for the simulated single-resonants while Figures 7(d), 7(e), and 7(f) show the corresponding results for the equivalents. Respectively, Figure 7(g) is for the multi-resonant dipole and (h) for the equivalent. In the multi-resonant equivalent each parallel-stage (i.e., RLC-circuit) is to perform the resonant wavemode where the resistance maximum happens. The combination of three stages models the entire multi-resonant structure such that the 1st is the lowest, and so forth. An interesting remark in Figure 7 is observed when comparing the results with Figure 6: the contact results (red dashed lines) for the single-resonant dipoles at 6 GHz and 9 GHz are not smaller with respect to the free space reference graph (black solid). This is obviously the situation because of the existence of the substrate causing the additional increase of 1.6 mm for D_{A-S} , thus resulting in the clearly higher relative increase within the range of reactive-near field in comparison with 3 GHz, which explains this difference. On the other hand, this is advantage for the wearable antenna at high frequency, since without the substrate the detuning were also stronger on contact with respect to free space than the shown shifts in Figure 4: 1050 MHz at 6 GHz and 1250 MHz at 9 GHz. Therefore, more detuning is required for the single-resonant antenna with high centre frequency

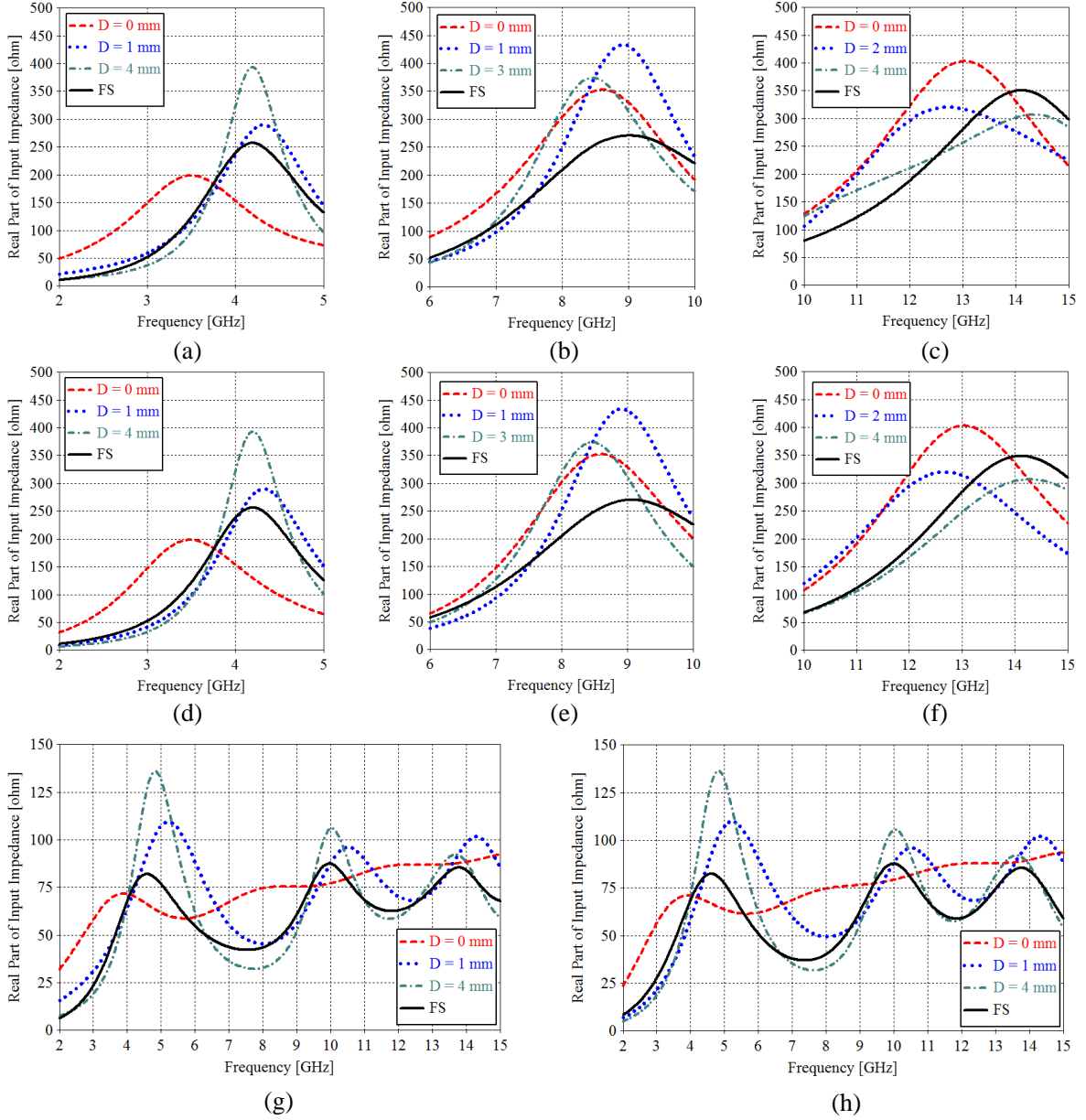


Figure 7. Antenna impedance behaviour in free space (FS), and at some distances on the tissue surface for single-resonant dipoles based on (a), (b), (c) antenna simulations ((a) at 3 GHz, (b) at 6 GHz, and (c) at 9 GHz) and (d), (e), (f) by equivalent circuits. Figure (g) shows the results for multi-resonant dipole and (h) corresponding positions for its equivalent.

if, e.g., the same antenna is aimed to use in free space and on-body. Based on the results shown in Figure 7, it is concluded that the used circuits can follow excellently the antenna impedance behaviour in the proximity of tissue. But how can be the behaviour in the proximity of tissue, introduced in Figure 6, physically explained, and what happens for the antenna (dimensions) in the said range, are discussed in the next part.

4.3. Physical Dipole Behaviour Based on Equivalent in the Vicinity of Tissue

Based on the definition of the circuit components for the parallel-stages of the defined lumped-element, the values for equivalents were collected and expressed in relation with the free space operation. In

other words, the reference point is simply defined to be in free space. Since the parallel-resonant stage is the combination of the capacitance C , inductance L and resistance R , the results of the changes within the reactive near-field are presented in the individual graphs by separated according to the said components. These are depicted in Figure 8 and the nominal (reference) values presented on Table 3.

It is understandable that the results in Figure 8 are not absolutely perfect to model the physical antenna behaviour in the proximity of tissue. But this method is observed to be very suggestive and exploitable for the understanding about the operation of the wearable broadband dipoles. Therefore,

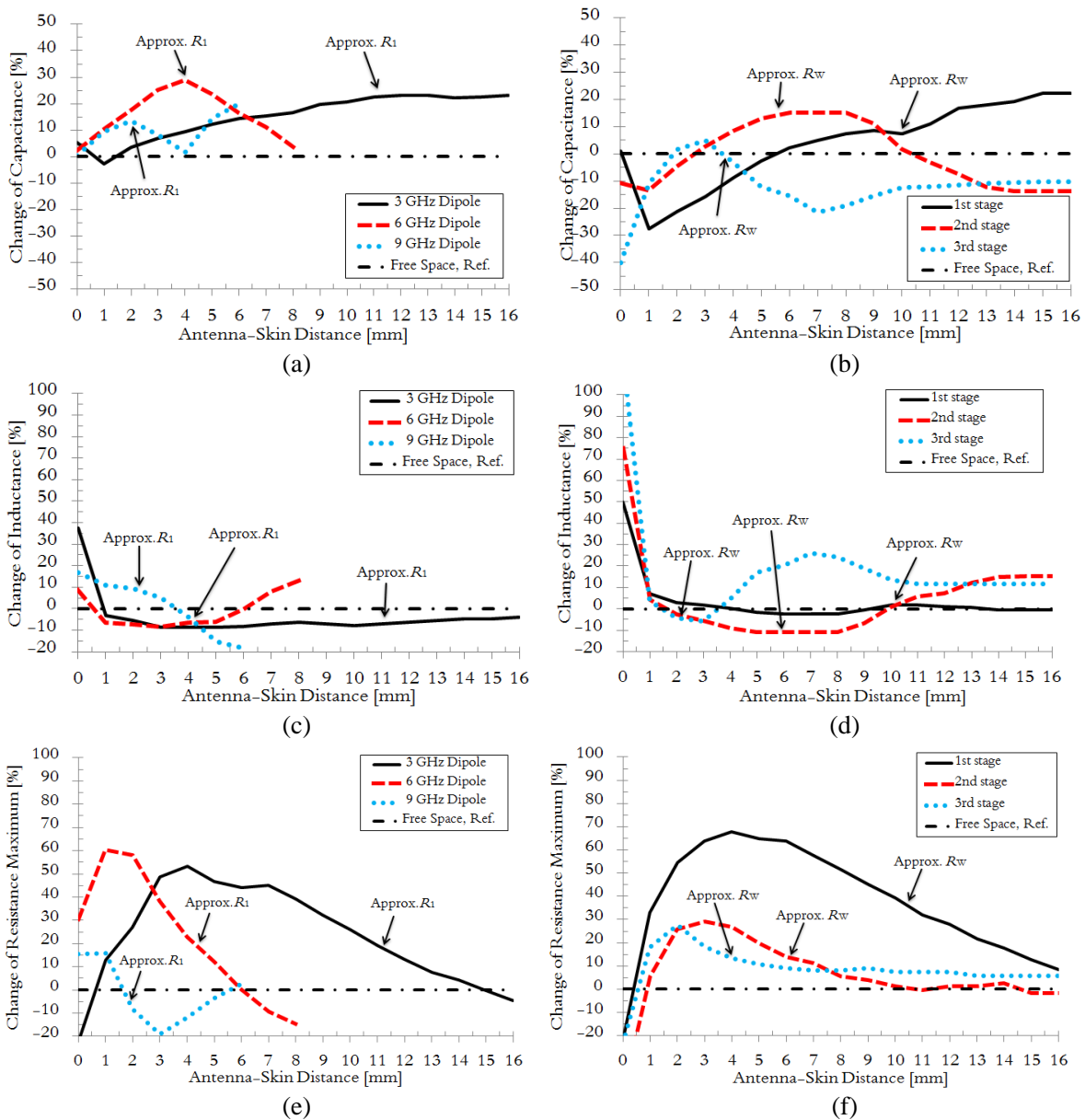


Figure 8. Variation of the relative changes of physical antenna characteristics expressed by equivalent circuit element values in terms of (a), (b) capacitance, (c), (d) inductance, and (e), (f) the maximum value of input resistance in comparison with the free space values in Table 3 as a function of antenna-tissue distance for (a), (c), (e) single and (b), (d), (f) multi resonant dipoles. Note that reference line (Free Space, Ref.) depicts the nominal value of free space values, which are used as the reference point to announce the relative changes. The calculated reactive near-field boundaries R_1 or R_W are indicated in graphs with the exception that the distance of a 1.6 mm thick substrate is taken into account.

Table 3. Element values of free space (reference) equivalent circuits for single and multi-resonant dipoles.

component	Single-resonant dipoles			component	multi-resonant dipole		
	3 GHz	6 GHz	9 GHz		stage: $n = 1$	stage: $n = 2$	stage: $n = 3$
C_1	0.43 pF	0.17 pF	0.09 pF	C_n	0.69 pF	0.82 pF	0.68 pF
L_1	3.38 nH	2.10 nH	1.36 nH	L_n	1.73 nH	0.31 nH	0.19 nH
R_1	256.55 Ω	270.26 Ω	348.71 Ω	R_n	80.09 Ω	70.50 Ω	71.00 Ω

the principal impedance behaviour can be acquired with this method. As well, it should be understood that these graphs show the required changes for the studied lumped-element circuit components in comparison with the free space values. The studied equivalent structure have been concluded to model accurately the dipole operation in free space, e.g., in [23, 32, 33, 35, 36].

As readable from the graphs, the closest use position that 1.6 mm thick substrate allows on-body, the significance of the capacitance is relatively minor with the inductance. This means that the total length of dipole, which has the connection to the inductance via reactance in (2), faces the stronger change in the proximity of lossy tissue than the width of dipole (resp. capacitance). Study in [35] supports this result. However, the capacitance cannot be the same as in free space as deductible from the result. When D_{A-S} is increased, the relative proportion of capacitance changes more than for the inductance, which remains rather constant with the higher distances, see Figures 8(a)–(d). This increase of circuit capacitance can be connected both to the mentioned variation of the circle in Smith's Chart and to the decrease of the achievable bandwidth in the middle of the reactive near-field boundary (as described in the previous section). This happens because the additional increase of the circuit capacitance is concluded to restrict the available bandwidth [23].

Even though the reactive near-field boundaries marked in Figure 8 are just approximations, some remarks can be stated of the physical operation of the studied antennas for the considered distances as:

- The capacitance having the connection with the width of dipole increase with D_{A-S} from on contact usage, and achieves the maximum value close to the reactive near-field boundary.
- The inductance having the connection with the length of dipole has the maximum value on contact, decrease strongly within the first millimetres with D_{A-S} and remains relatively constant further.
- The maximum value of R_{in} is observed to clearly increase with D_{A-S} , to have the maximum in the first third of the studied range, descending close to free space behaviour at the boundary.

These results show the advantage of using equivalent circuits for the analysis of antenna physical behaviour. To our best knowledge, this is the first time to present these effects for the physical broadband dipole operation in the reactive near-field range. In addition, the content of the results can be extended since we used the traditional dipoles for investigations. Most antennas can be analysed based on dipoles, for instance, the widely used monopole and patch antennas for the wearable usage.

Based on the results for the antenna physical behaviour in Figure 8, the impact of tissue within the reactive near-field for the broadband dipoles can be taken into account by adding parasitic components parallel with the circuit resonator structures of free space values. The proposed final equivalent circuit is presented in Figure 9, which includes the proportion of tissue shown with black dashed rectangular boxes. Grey dashed lines with arrows indicate the connection of the parasitic components introduced by tissue with the free space equivalent. In order to understand the total circuit concept extensively, some observations can be highlighted.

As the dipole can be illustrated below the first resonant frequency by capacitor [35], the capacitance of the series-resonant is hence associated with the antenna reactance (for the single-resonant by C_0 and for multi-resonant by C_0 and C_4). Thus, the entire series part (i.e., the combination of C and L resonates) mainly defines the antenna reflection coefficient S_{11} , i.e., matching as we have shown in [23]. In addition, it has the impact on the reactance of input impedance. This is understandable, since the series part directly defines the resonant frequency for antenna, but the changes are not visible to vary the real part of input impedance. However, the series part changes the antenna reactance, which is

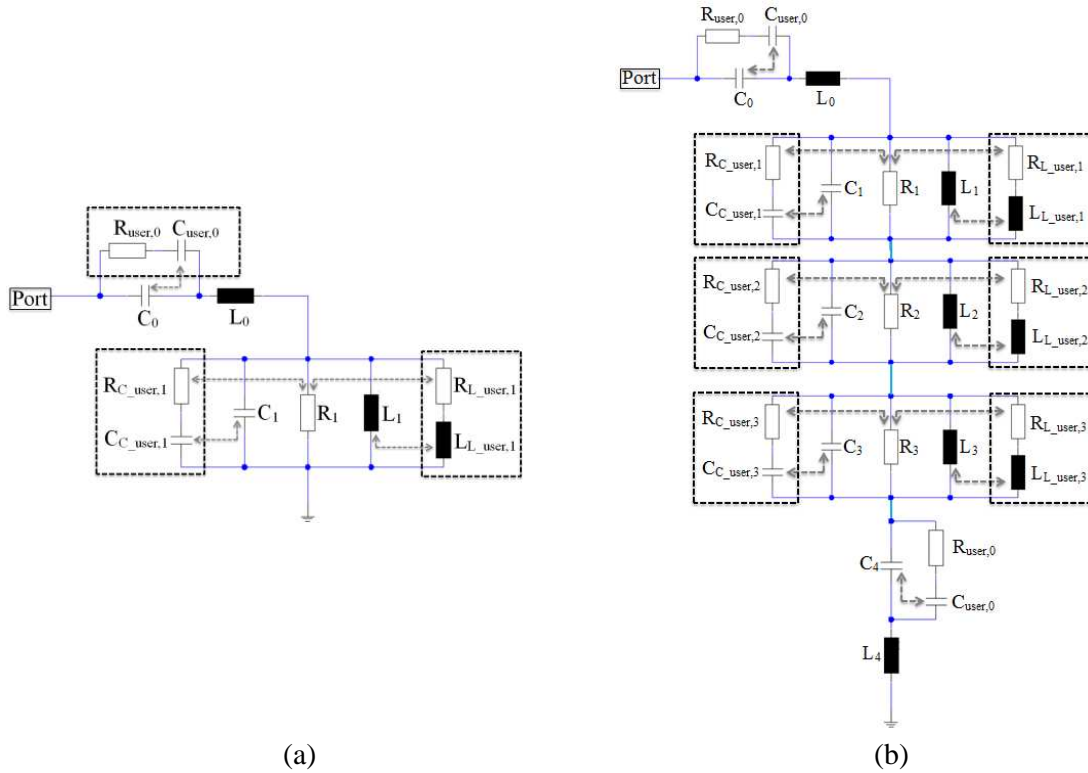


Figure 9. Final equivalent circuit for (a) single-resonant dipole, and (b) multi-resonant dipole indicating the proportion of tissue by parasitic components inside the black dashed rectangular boxes and the connection between the free space components with additional parasitic to form the final physical behaviour by grey dashed arrows.

assumed to cause the changes for the resonances. The parallel stage(s) is to define the RLC -resonance in the situation the dipole reactance is close to zero and the series-resonance is in the target frequency, while R_r for dipole defined in (2) (i.e., 73 ohm for ideal dipole) can be read from the parallel resistance graph at the resonant frequency of the series-part. In the proximity of tissue, the resonance frequencies are detuned downwards according to the perturbation theory in [24]. The detuning is shown for resistor via becoming more inductive as in [35], introducing parasitic capacitance in parallel with the capacitor as in [25], and both are associated with the electric fields. This is because the introduced dielectric material changes the component permittivity such that capacitances are multiplied and resistors divided with the permittivity of the surroundings. By associating these to the attribute, the following remarks can be stated:

- The higher is ϵ_r of tissue (note the strong variation of permittivity with the frequency) or the smaller the D_{A-S} on tissue, the higher is the addition of the capacitance in total to the series part.
- The smaller the D_{A-S} , the stronger is the change of resonant frequency, i.e., change in S_{11} , as well for R_{in} and X_{in} .
- Only the resonance peak of the maximum value of resistance R_{in} changes with the higher D_{A-S} , but the reactance X_{in} is observed to change at all frequencies, i.e., throughout the simulated bandwidth. Note also the connection of X_{in} with the length of the dipole.
- The losses of tissue have an impact on the parallel and series stages, and are placed in parallel with free space components in series with the capacitance or inductance.
- The losses introduced by tissue describe the proportion of loss resistance R_L in (3), which improves or attenuates the resonance of LC -circuit. For instance, on contact the improved matching is visible but is observed to deteriorate with the D_{A-S} , and tissue causes the resistor to appear more inductive.

5. CONCLUSION AND FUTURE WORK

The present paper considered the impact of tissue on the wearable antenna operation in the range of the reactive near-field. The variations of parameter in terms of efficiency, current distributions and antenna impedance in the mentioned range were demonstrated and compared with the theoretical boundaries. We considered the variations of broadband dipole equivalent circuit operation in comparison with the data extracted from simulations, and separated the effect of capacitance, inductance and resistance on practical antenna dimensions within the range of the reactive near-field. Based on the observations, we proposed parasitic components to take into account the impact of tissue on wearable broadband antenna operation. The first time the antenna impedance behaviour was presented in terms of capacitance, inductance and resistance as a function of the radiator distance on the tissue surface for ultra wideband (UWB) antennas. We found that the capacitance with the connection of the width of a dipole increases with the distance by achieving the maximum value close to the reactive near-field boundary. The inductance with the connection of the dipole length was observed to have the maximum value on contact tissue, decreasing strongly with the first millimetres then remaining constant further. Input resistance maximum value was observed to clearly increase with the distance, having the maximum in the first third of the studied range finally descending close to the value in free space at the boundary.

The results of this study increase the knowledge of the antenna impedance behaviour in comparison with the practical antenna dimension in the vicinity of tissue. This is particularly important understand for the broadband antennas, which are used without the matching components. After understanding the influence of antenna impedance on dimensions, matching can be maximised on-body. The presented impedance behaviour as a function of the distance on the tissue surface assists to choose the optimal distance for a wearable antenna, which is matched in free space. In addition, analysing the behaviour indicates how a body impacts on the operation of an antenna that is aligned for some distance on the tissue surface. The effect on impedance can be compensated at the end by changing the antenna dimensions, as demonstrated in the earlier study by authors' in [23].

These results can be extended in many ways. It is recommended to derive corresponding evaluations for the other antenna types as widely used monopole and patch antennas, since the operation can be compared with the results presented in this paper. Alternatively, the investigations of bendable wearable antenna characteristics by using equivalents are highly suitable in order to understand the physical effect of bending the radiator on impedance behaviour. As well, it is proposed to apply the content of this paper to the practical antenna design work on-body, since there is the clear connection.

ACKNOWLEDGMENT

This work was supported in part by the Finnish Funding Agency for Technology and Innovations (Tekes) through Enabling Wireless Healthcare Systems (EWiHS) project and Infotech Oulu Doctoral Program, Centre for Wireless Communications, and University of Oulu, Finland. Also Nokia foundation is appreciated of financial support of the research work for first author.

REFERENCES

1. Hall, P. S. and Y. Hao, *Antennas and Propagation for Body-centric Wireless Communications*, 2nd Edition, Artech House, Norwood, 2012.
2. "IEEE standard for local and metropolitan area networks," IEEE 802.15.6-2012 — Part 15.6: Wireless Body Area networks, 2012.
3. Sankaranlingam, S. and B. Gupta, "Development of textile antennas for body wearable applications and investigations on their performance under bent conditions," *Progress In Electromagnetics Research B*, Vol. 22, 53–71, 2010.
4. Vorobyov, A. and A. Yarovoy, "Human body impact on UWB antenna radiation," *Progress In Electromagnetics Research M*, Vol. 22, 259–269, 2012.
5. Kivekäs, O., T. Lehtiniemi, and P. Vainikainen, "On the general energy-absorption mechanism in the human tissue," *Microw. Opt. Tech. Lett.*, Vol. 43, No. 3, 195–201, Nov. 2005.

6. Klemm, M. and G. Troester, "EM energy absorption in the human body tissues due to UWB antennas," *Progress In Electromagnetics Research*, Vol. 62, 261–280, 2006.
7. Tuovinen, T., M. Berg, K. Y. Yazdandoost, and J. Iinatti, "Ultra wideband loop antenna on contact with human body tissues," *IET Proceedings — Microwaves Antennas and Propagation*, Vol. 7, No. 7, 588–596, Mar. 2013.
8. Christ, A., A. Kligenböck, T. Samaras, C. Goiceanu, and N. Kuster, "The dependence of electromagnetic far-field absorption on body tissue composition in the frequency range from 300 MHz to 6 GHz," *IEEE Trans. Microw. Tech.*, Vol. 54, No. 5, 2188–2195, May 2006.
9. Tuovinen, T., T. Kumpuniemi, K. Y. Yazdandoost, M. Hämäläinen, and J. Iinatti, "Effect of the antenna-human body distance on the antenna matching in UWB WBAN applications," *Proc. 7th Int. Symp. Med. Inform. Commun. Technol. (ISMICT2013)*, 1–5, Japan, Mar. 2013.
10. Alomainy, A., Y. Hao, and D. M. Davenport, "Parametric study of wearable antennas with varying distances from the body and different on-body positions," *IET Seminar on Antennas Propag. for Body-Centric Wireless Commun.*, 84–89, London, UK, Apr. 2007.
11. Kaivanto, E., M. Berg, E. Salonen, and P. Maagt, "Wearable circularly polarized antenna for personal satellite communication and navigation," *IEEE Trans. Antennas Propag.*, Vol. 53, No. 124, 4490–4496, Dec. 2005.
12. Koohestani, M., N. Pires, A. K. Skrivervik, and A. A. Moreira, "Performance study of a UWB antenna in proximity to a human arm," *IEEE Antennas Wireless Propag. Lett.*, Vol. 12, 555–558, 2013.
13. Sani, A., A. Alomainy, J. Santas, and Y. Hao, "Time domain characterization of ultra wideband wearable antennas and radio propagation for body-centric wireless networks in healthcare applications," *Proc. Int. Summer School and Symp. Med. Dev. Biosensors (ISSS-MDBS)*, 129–132, Hong Kong, Jun. 2008.
14. Balanis, C. A., *Antenna Theory Analysis and Design*, 3rd Edition, John Wiley & Sons, 2005.
15. Stutzman, W. L. and G. A. Thiele, *Antenna Theory and Design*, 2nd Edition, John Wiley & Sons, 1998.
16. Wheeler, H. A., "The radiansphere around a small antenna," *Proc. the Inst. Radio Eng. (IRE)*, 1325–1331, 1959.
17. Räsänen, A. V. and A. Lehto, *Radio Engineering for Wireless Communication and Sensor Applications*, Artech House, Norwood, 2003.
18. Tuovinen, T., M. Berg, and E. Salonen, "The comparative analysis of UWB antennas with complementary characteristics: A functionality in FS and applicability for the usage close to tissues," *PIERS Proceedings*, 134–138, Stockholm, Sweden, Aug. 12–15, 2013.
19. "Revision of Part 15 of the commission's rules regarding ultra wideband transmission systems," FCC Notice of Proposed Rule Making, ET-Docket 98-153, FCC 02-48, 2002.
20. Oppermann, I., M. Hämäläinen, and J. Iinatti, *UWB Theory and Applications*, John Wiley & Sons, England, 2004.
21. "Computer simulation technology microwave studio software," Online Available: <http://www.cst.com>.
22. Chen, Z. N., *Antennas for Portable Devices*, John Wiley & Sons, 2007.
23. Tuovinen, T. and M. Berg, "Impedance dependency on planar broadband dipole dimensions: an examination with antenna equivalent circuits," *Progress In Electromagnetics Research*, Vol. 144, 249–260, 2014.
24. Harrington, R. F., *Time-harmonic Electromagnetic Fields*, McGraw-Hill, 1961.
25. Alves, T. M., B. Poussot, and J.-M. Laheurte, "Analytical propagation modeling of BAN channels based on the creeping-wave theory," *IEEE Trans. Antennas Propag.*, Vol. 57, No. 4, 1269–1274, Apr. 2011.
26. Sánchez-Hernández, D. A., *High Frequency Electromagnetic Dosimetry*, Artech House, 2009.
27. Holopainen, J., R. Valkonen, O. Kivekäs, J. Ilvonen, L. Martinez, P. Vainikainen, J. R. Kelly, and P. S. Hall, "Equivalent circuit model-based approach on the user body effect of a mobile terminal

- antenna,” *Proc. Loughborough Antennas Propag. Conf. (LAPC)*, 217–220, UK, 2010.
28. Barnes, F. S. and B. Greenebaum, *Bioengineering and Biophysical Aspects of Electromagnetic Fields*, 3rd Edition, Taylor & Francis Group, Boca Raton, 2007.
 29. Gandhi, O. P., B. Q. Gao, and J. Y. Chen, “A frequency-dependent finite-difference time-domain formulation for general dispersive media,” *IEEE Trans. Antennas Propag.*, Vol. 41, No. 4, 658–665, Apr. 1993.
 30. Wang, Y., J. Z. Li, and L. X. Ran, “An equivalent circuit modeling method for ultra-wideband antennas,” *Progress In Electromagnetics Research*, Vol. 82, 433–445, 2008.
 31. Ansarizadeh, M. and A. Ghorbani, “An approach to equivalent circuit modeling of rectangular microstrip antennas,” *Progress In Electromagnetics Research B*, Vol. 8, 77–86, 2008.
 32. Li, R. L., W. Terence, B. Pan, K. Lim, J. Laskar, and M. M. Tentzeris, “Equivalent-circuit analysis of a broadband printed dipole with adjusted integrated balun and an array for base station applications,” *IEEE Trans. Antennas Propag.*, Vol. 57, No. 7, 2180–2184, Jul. 2009.
 33. Hamid, M. and R. Hamid, “Equivalent circuit of dipole antenna of arbitrary length,” *IEEE Trans. Antennas Propag.*, Vol. 45, No. 11, 1695–1696, Nov. 1997.
 34. Holopainen, J., R. Valkonen, O. Kivekäs, J. Ilvonen, and P. Vainikainen, “Broadband equivalent circuit model for capacitive coupling element-based mobile terminal antenna,” *IEEE Antennas Wireless Propag. Lett.*, Vol. 9, 716–719, 2010.
 35. Liao, Y., T. H. Hubing, and D. Su, “Equivalent circuit for dipole antennas in a lossy medium,” *IEEE Trans. Antennas Propag.*, Vol. 60, No. 8, 3950–3953, Aug. 2012.
 36. Tang, T. G., Q. M. Tien, and M. W. Gunn, “Equivalent circuit of a dipole antenna using frequency-independent lumped elements,” *IEEE Trans. Antennas Propag.*, Vol. 41, No. 1, 100–103, Jan. 1993.